Prediction of fluid occupancy in fractures using network modeling and x-ray microtomography. II: Results

Mohammad Piri*
Department of Chemical and Petroleum Engineering, University of Wyoming, Laramie, Wyoming 82071-2000, USA

Zuleima T. Karpyn
Department of Energy and Mineral Engineering, The Pennsylvania State University, University Park, Pennsylvania 16802-5000, USA
(Received 25 November 2006; published 31 July 2007)

This paper presents the implementation of the pore-scale network model described in paper I [see preceding paper, Z. T. Karpyn and M. Piri, Phys. Rev. E **76**, 016315 (2007)]. The model is used to estimate flow properties and predict fluid occupancy during two-phase flow displacements in a rough-walled fracture. The fracture's inner structure is available from the reconstruction of x-ray microtomography images of a fractured sandstone core. The model is able to represent mechanisms such as pistonlike displacement, cooperative pore filling, and snapoff. We study the effects of aperture map scales, rate of injection, and gravity on the distribution of phases inside the fracture and present successful predictions of fluid occupancy during primary drainage, imbibition, and secondary drainage. Results were validated rigorously against x-ray microtomography scans obtained from two-phase flow experiments [see Z. T. Karpyn, A. S. Grader, and P. M. Halleck, J. Colloid Interface Sci. **307**, 181 (2007)] and showed two-phase fluid structures in agreement with experimental observations.

DOI: 10.1103/PhysRevE.76.016316 PACS number(s): 47.56.+r, 47.80.Jk, 91.60.Ba

I. INTRODUCTION

Naturally fractured reservoirs are typically modeled using dual-porosity representations [1–5] in which straight-line relative permeabilities ($k_{ri}=S_i$) and zero capillary pressures ($P_{cf}=0$) are commonly assigned to the fracture domain. These simplifications, originally proposed by Romm [6], can lead to significant errors in recovery predictions [1,7–9]. Straight-line relative permeabilities are consistent with the representation of flow through smooth parallel plates. However, real fractures exhibit roughness and complex aperture variations that create tortuous paths of flow. In order to create reservoir models with more accurate fracture representations, it is essential to determine characteristic fracture flow properties capturing the intricate relationship between fracture geometry and fluid flow.

In this work, we present a pore-scale network model of a single fracture, whose void structure had been mapped using x-ray microtomography. We examine the relevance of scale effects, viscous and gravity forces on the predictive capabilities of the model, and compare modeled multiphase flow structures of wetting and nonwetting phases against x-ray microtomography data. Fracture relative permeabilities and capillary pressures are also presented in this paper. Results from this work provide valuable insight into the complex flow characteristics of real fractures. Details of the x-ray microtomography and the network model are presented in paper I [10].

II. PRIMARY DRAINAGE

Here the modeling results for primary drainage are presented. We use a capillary dominated invasion percolation approach [11]. Oil is injected from the inlet, left side of rectangles shown in Fig. 1, into a fracture that is fully saturated with water (no trapped air) while the defending phase, water, is allowed to escape the network only from the outlet. A cluster of the defending phase is considered trapped when it is not continuous to the outlet. First, the generic behavior is studied, and then the fluid occupancy predicted by the model is compared against its experimental counterpart.

A. Generic results

Primary drainage was carried out using $\theta_{ow}=10°$ and $\sigma_{ow}=41.2$ mN/m (see Ref. [12]). All the displacements were allowed to take place reducing water saturation to less than 1%. Water is always connected to the outlet through the wetting layers. Figure 1 shows fluid occupancy at different water saturations. Oil, in dark gray, first invades the larger elements located at the inlet, lower side, and outlet of the fracture (see Fig. 11 in Ref. [10] for the location of large elements). Then, oil continues to displace water from the smaller accessible elements and generate the occupancy patterns seen in Fig. 1.

Figures 1(a)–1(c) show the preferential progression of oil along the edges of the fracture. This is due to the presence of larger apertures and thus smaller threshold capillary pressures.

Figures 2(a) and 2(b) present computed relative permeability and capillary pressure. Oil percolates the network at $S_w\approx0.67$ where it shows a relative permeability of about 0.15. Water relative permeability exhibits a sharp drop at 0.9 to 0.8 water saturation range. This is attributed mainly to the channel of oil-filled elements connecting the upper and lower sides of the fracture; see Figs. 1(a) and 1(b). This channel blocks the flow of water causing a sharp drop in the water conductivity of the network. One may find it interesting that water relative permeability drops to smaller than 0.01 only

*mpiri@uwyo.edu

(a) $S_w = 0.9085$

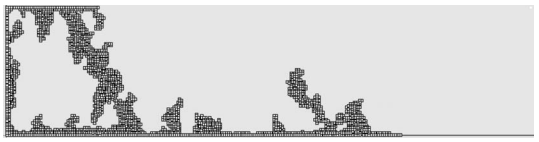

(b) $S_w = 0.8061$

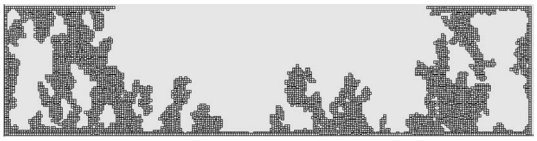

(c) $S_w = 0.5871$

(d) $S_w = 0.3641$

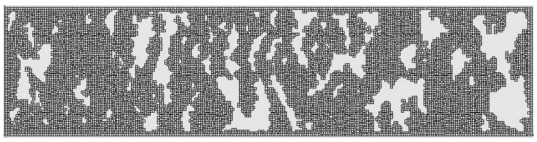

(e) $S_w = 0.1878$

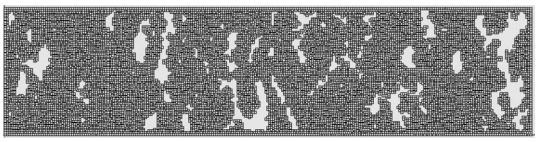

(f) $S_w = 0.1057$

FIG. 1. Modeling results—fluid occupancy at different water saturations during primary drainage using map C (see Table II in Ref. [10]). Dark gray elements are occupied by the invading phase (oil) while the light gray areas include elements that are fully saturated with the defending phase (water).

by 53% reduction in its saturation. This is mainly due to the fact that most of the large, highly conductive elements are already filled by oil which blocks the flow of water significantly.

B. Comparison against the experiment

In order to compare fluid occupancies predicted by the network model to those mapped experimentally, we conducted a primary drainage simulation using the same interfacial tension and contact angle as before, see Sec. II A, allowing water saturation to reduce to the same water saturation

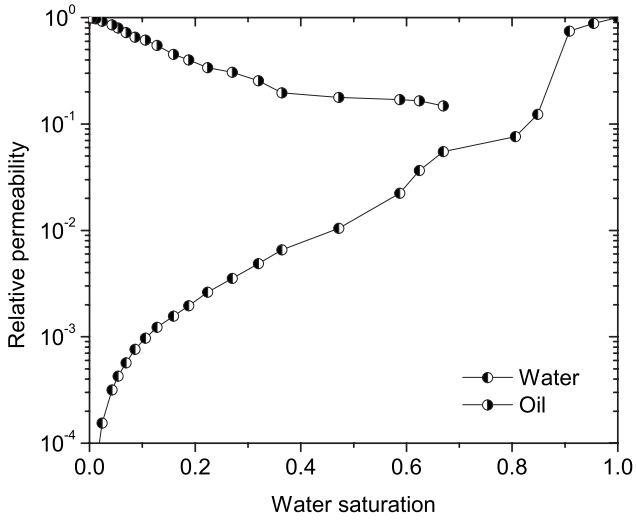

(a) Relative permeability, truncated at 1×10^{-4}

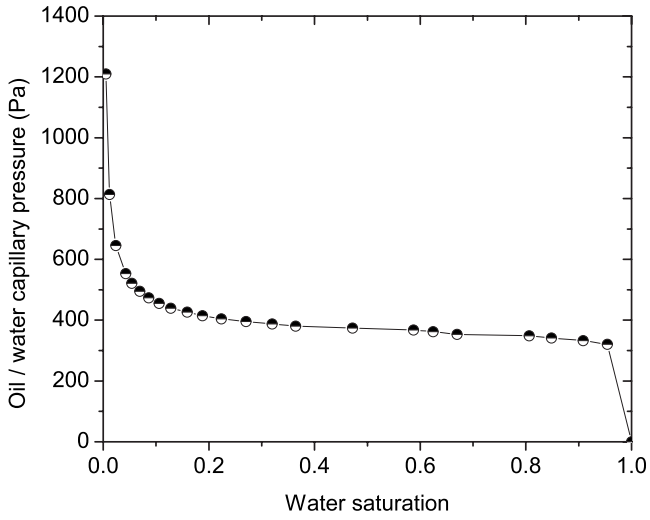

(b) Capillary pressure

FIG. 2. Modeling results—oil-water relative permeability and capillary pressure for primary drainage using map C (see Table II in Ref. [10]); $S_{wirr} \approx 0.005$. See Fig. 5(a) for fluid occupancy at irreducible water saturation (S_{wirr}).

reported experimentally, 0.35. This is the water saturation that was measured at the end of stage 3 of the experiment (see Table I in Ref. [10]). Since only the fluid occupancy is compared, we force the model to terminate the displacement at S_w=0.35 without necessarily waiting for the new capillary equilibrium.

Figure 3(a) exhibits a top view of the fluid occupancy generated by x-ray computed tomography (CT) imaging at the end of primary drainage (stage 3 of the experiment) while Figs. 3(b)–3(e) show predicted fluid occupancy using four networks with different resolutions, i.e., different number of elements. These four networks (A to D) were generated using the coarse aperture maps and resolutions listed in Table II of Ref. [10]. Even though the model uses entirely conceptual networks of connected pores and throats it is capable of *predicting* the fluid occupancy generated by the experiment. Al-

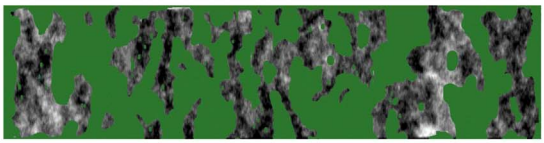

(a) (Color online) Experiment, $S_w = 0.35$, dark and light gray areas show water-filled elements while green elements are occupied by oil.

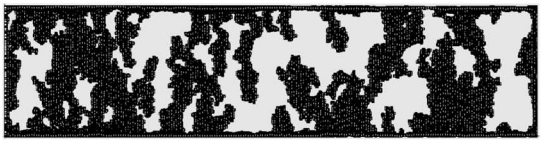

(b) Modeling results using map A, $S_w = 0.3498$

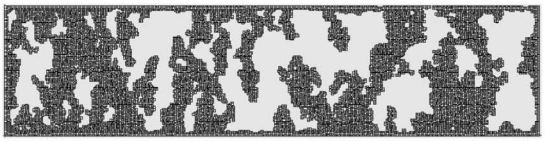

(c) Modeling results using map B, $S_w = 0.351$

(d) Modeling results using map C, $S_w = 0.3505$

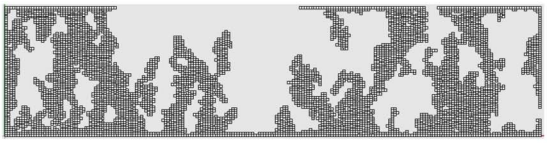

(e) Modeling results using map D, $S_w = 0.3501$

FIG. 3. (Color online) Comparison against the experiment (primary drainage)—experimental and predicted fluid occupancies at $S_w \approx 0.35$. Predicted fluid occupancies [(b) to (e)] were generated using coarse maps A, B, C, and D (see Table II in Ref. [10]), respectively, where dark gray elements are occupied by the invading phase (oil) while the light gray areas include elements that are fully saturated with the defending phase (water).

most all the features of the fluid occupancy seen in the x-ray image have been reproduced by the model using networks A, B, and C. Reducing the resolution to those of coarse maps A, B, and C did not affect the quality of the prediction. However, as it is seen in Fig. 3(e), network D fails to reproduce a correct fluid occupancy at the upper side of the fracture. The discrepancy observed in network D is purely a resolution effect. The algorithm we utilize to coarsen the original high-resolution map (OHRM) is not able to conserve the topological features of the original aperture map when resolution was reduced significantly. Consequently, we decided to use map C for the rest of the modeling results presented in this paper. Also, using map C is computationally less expensive, compared to maps A and B.

Figure 4 presents a more rigorous comparison of predicted fluid occupancy against experimental data. We take CT slices at different locations, along the length of the fracture, and compare them with the fluid occupancy predicted by the model for the same locations. This is done for eight different locations. Agreement between fluid occupancy predicted by the model and those given by the corresponding CT slices is excellent. This indicates that the capillary dominated flow assumption is valid for primary drainage in this experiment.

One should note that every CT image presents fluid occupancy in a slice of the core that is only 0.032 548 mm thick (see Table II in Ref. [10]), while the network resolutions we have used are lower. This means that every row of elements in the predicted fluid occupancy corresponds to several adjacent CT slices. However, this does not adversely affect the quality of the aforementioned agreement between predicted and experimental fluid occupancies.

III. IMBIBITION

Injection of water into oil (imbibition) is modeled after primary drainage. We study both capillary dominated and quasidynamic flow for which rate and gravity effects are taken into account. In this section we present general results for both cases and then compare the results of our simulations against their experimental counterparts.

A. Capillary dominated

In capillary dominated simulations, flow rate and gravity effects are ignored. We use $\theta_{\mathrm{ow}}^{a}=25°$ and $\sigma_{\mathrm{ow}}=41.2$ mN/m (see Ref. [12]) and start from irreducible water saturation, $S_{\mathrm{wi}}=0.0046$, reached during primary drainage; see Fig. 5(a). Water injection is continued until all the remaining oil is trapped; i.e., residual oil saturation is reached. Table I lists the number of different displacement mechanisms taking place. A nonzero advancing oil-water contact angle and large apertures make the number of snapoff displacement small in comparison to the number of pistonlike and cooperative pore filling displacements. This means that trapping of the nonwetting phase is mainly due to the displacements by MTM rather than by AMs.

Figure 5 shows the progression of fluid occupancy at different water saturations during imbibition. Since snapoff does not have a major role in developing the flow pattern, the cooperative pore filling is the displacement mechanism that determines the fluid occupancy. Initially snapoff displacements form some water-filled elements providing sites from which pistonlike displacements or cooperative pore filling events may be initiated. When such sites are available water invasion may take place in smaller oil-filled elements and is favored when greater number of neighboring elements are filled with the wetting phase.

Relative permeability and capillary pressure for imbibition are shown in Figs. 6(a) and 6(b). Residual oil saturation is 0.4827 where maximum water relative permeability reaches 0.2161. Residual oil is left in larger pores forming 77 trapped clusters with 7827 member elements that hold trapped oil in the center.

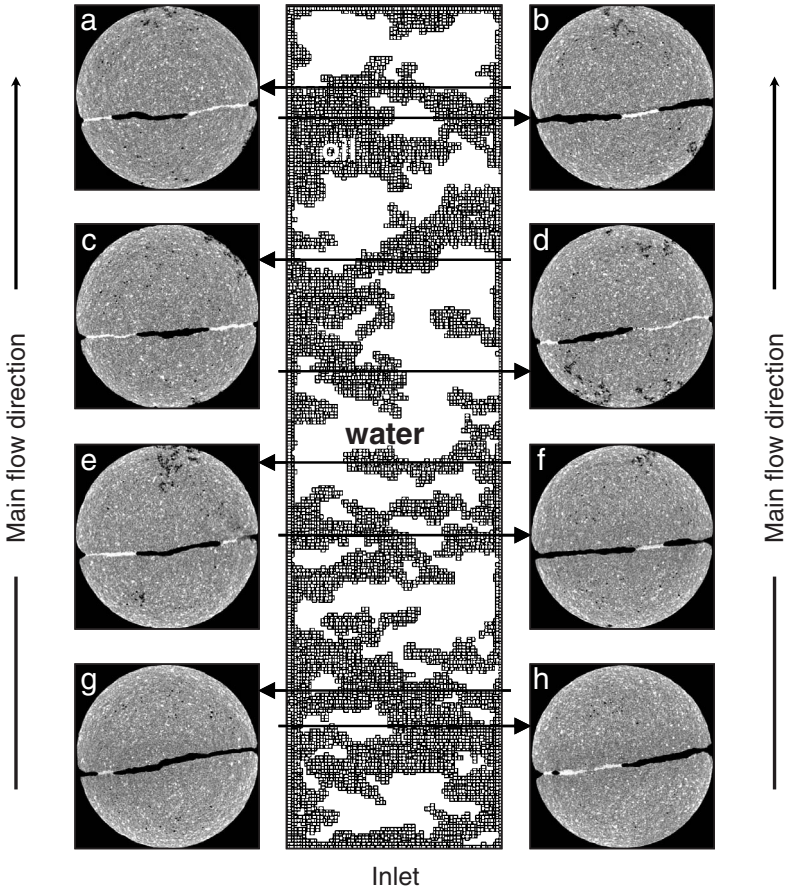

FIG. 4. Comparison against the experiment (primary drainage)—comparison of predicted fluid occupancy against experimental CT slices at $S_w \approx 0.35$, using map C (see Table II in Ref. [10]). Distance from the bottom, or inlet, of the core: (a) 92.18 mm; (b) 88.46 mm; (c) 71.18 mm; (d) 56.63 mm; (e) 46.35 mm; (f) 37.85 mm; (g) 18.97 mm; (h) 14.06 mm. In the predicted fluid occupancy, dark gray elements are occupied by the invading phase (oil) while the light gray areas include elements that are fully saturated with the defending phase (water). In the CT slices, white represents water while black represents oil.

B. Rate effects

In this section, we present modeling results for quasidynamic modeling of imbibition when rate effects are taken into account. The capillary number is varied by changing water flow rate in order to study its effects on the amount of residual oil saturation and maximum water relative permeability. The capillary number is given by

$$N_{\mathrm{Ca}} = \frac{Q_w \mu_w}{\bar{a} R_w N_w \sigma_{ow}}, \tag{1}$$

where Q_w and μ_w are the volumetric flow rate and the viscosity of water, respectively, $\bar{a}$ is the average aperture, R_w and N_w are the resolution and the number of elements along the width of fracture, and σ_{ow} is the oil-water interfacial tension.

Similar to Hughes and Blunt [13], and as discussed in Ref. [1], the most favorable displacement is the one for which the difference between the water pressure drop, from inlet to the element, and the threshold capillary pressure of the relevant displacement, in that element, is the smallest. Pressure drop in the oil phase and gravity effects are ignored.

Figure 7 shows fluid occupancy at the end of imbibition for different capillary numbers. Initial water saturation and parameter λ (see Ref. [10] for definition of parameter λ) for all cases were 0.024 and 2940, respectively. It is shown that the higher the capillary number is, the lower the residual oil saturation will become. When the capillary number is high, viscous forces become dominant over capillary forces, meaning that the magnitude of the water pressure drop from the inlet to a given element is greater than the threshold capillary pressure for the displacement in that element. This in turn means that displacements closer to the inlet are favored over displacements away from the inlet which translates into the

TABLE I. Number of different displacements taking place during capillary dominated imbibition.

Displacement type	Number of displacements
Snapoff	114
I_1 (pistonlike displacement)	1578
I_2	8785
I_3	2583

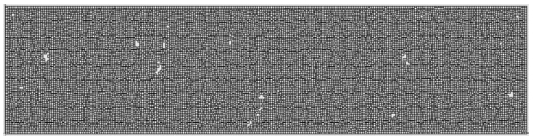

(a) $S_o = 0.9954$. One should note that the number of water-filled elements is zero at this saturation meaning that light gray areas show the asperities.

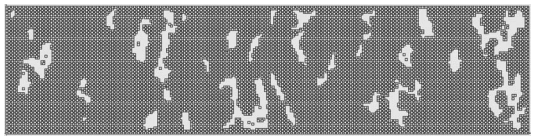

(b) $S_o = 0.9023$

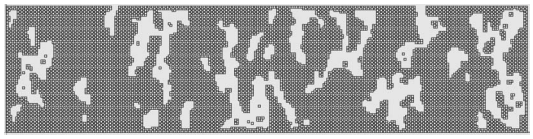

(c) $S_o = 0.801$

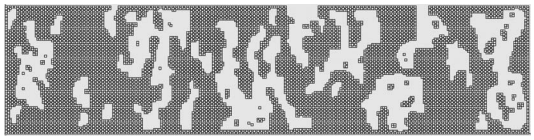

(d) $S_o = 0.7052$

(e) $S_o = 0.5846$

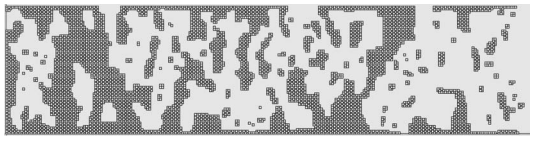

(f) $S_{or} = 0.4827$

FIG. 5. Modeling results—fluid occupancy at different oil saturations during capillary dominated imbibition using map C (see Table II in Ref. [10]). The dark gray elements are occupied by the defending phase (oil) while the light gray areas include elements that are fully saturated with the invading phase (water). Initial water and residual oil saturations were S_{wi}=0.0046 and S_{or}=0.4827, respectively.

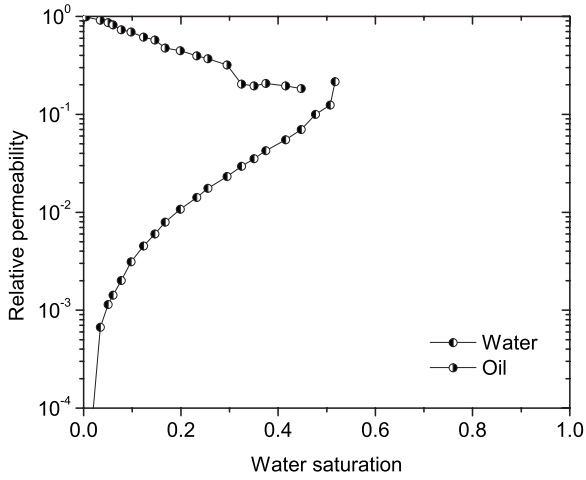

(a) Relative permeability, truncated at 1×10^{-4}. The last three data points for oil relative permeability are not shown as they are zero.

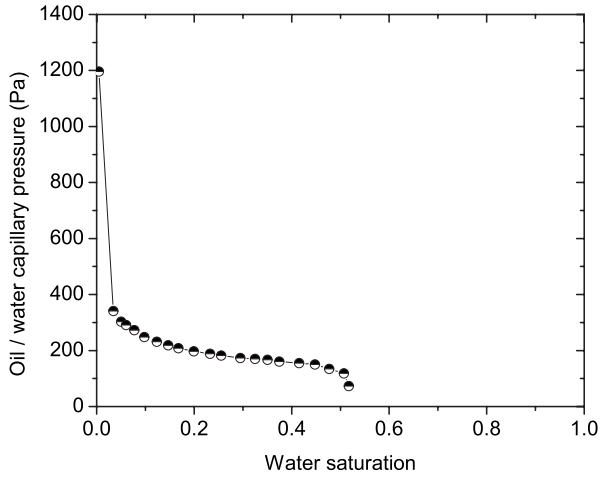

(b) Capillary pressure

FIG. 6. Modeling results—oil-water relative permeability and capillary pressure for capillary dominated imbibition using map C (see Table II in Ref. [10]). Initial water and residual oil saturations were S_{wi}=0.0046 and S_{or}=0.4827.

formation of a rather flat displacement front, see Fig. 9, reducing the chance of bypassing oil-filled elements and thus the possibility of trapping the oil phase. For small capillary numbers, however, the pressure drop from the inlet to a given element is smaller than the threshold capillary pressure of water displacing oil in that element making the displacement very similar to the capillary dominated case discussed in Sec. III A; cf. Figs. 5(f) and 7(f). For intermediate capillary numbers, there is a competition between viscous and capillary forces resulting in residual oil saturations that range from 0.0013 to 0.4841 and maximum water relative permeabilities that vary from 0.995 to 0.0335 (see next paragraph).

Figures 8(b) and 8(a) present the variation of residual oil saturation and maximum water relative permeability with respect to changes in capillary number. Residual oil saturation for $N_{Ca}=1\times10^{-3}$ is almost zero due to the frontal advance discussed earlier; see Fig. 7(a). When the capillary number is reduced to 1×10^{-4}, some of the very large elements located mainly along the upper and lower sides of the fracture remain oil filled, due to very low threshold capillary pressures, which eventually get trapped as the neighboring elements are filled with water; see Fig. 7(b). There is a significant increase in the amount of residual oil saturation when N_{Ca} is reduced from 1×10^{-4} to 1×10^{-5}; cf. Figs. 7(b) and 7(c). This is

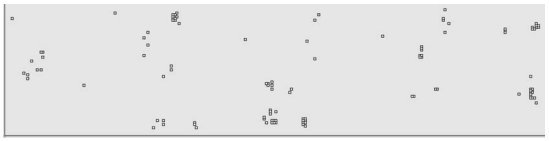

(a) $N_{Ca}=1\times10^{-3}$, $S_{or}=0.0013$

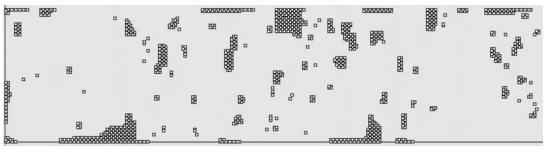

(b) $N_{Ca}=1\times10^{-4}$, $S_{or}=0.104$

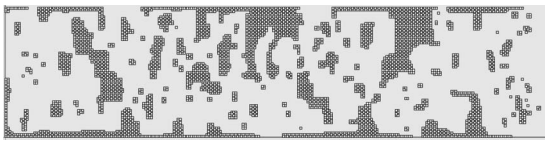

(c) $N_{Ca}=1\times10^{-5}$, $S_{or}=0.3582$

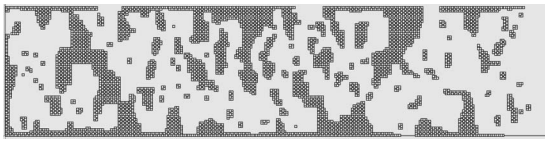

(d) $N_{Ca}=1\times10^{-6}$, $S_{or}=0.4289$

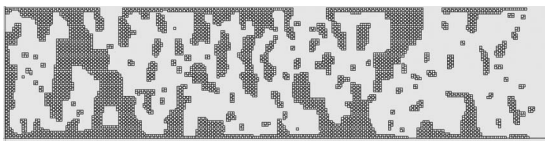

(e) $N_{Ca}=1\times10^{-7}$, $S_{or}=0.4556$

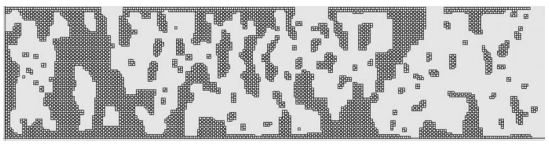

(f) $N_{Ca}=1\times10^{-8}$, $S_{or}=0.4841$

FIG. 7. Modeling results—effects of capillary number (N_{Ca}) on residual oil saturation of quasidynamic imbibition. Fluid occupancy at residual oil saturation for different capillary numbers using maps C (see Table II in Ref. [10]) with $S_{wi}=0.024$, $\lambda=2940$, and $\zeta=0°$. The dark gray elements are occupied by the defending phase (oil) while the light gray areas include elements that are fully saturated with the invading phase (water).

largely because small accessible elements, away from the inlet, get invaded by water, as N_{Ca} is not very high, increasing the possibility of bypassing large oil-filled elements to form trapped oil clusters. Further reduction in capillary number intensifies this process, as capillary forces become dominant, making the distance from the inlet less important. This expands to other locations in the network, see Figs. 7(d) and 7(f), eventually increasing the residual oil saturation to the level that was reported for the capillary dominated simulation.

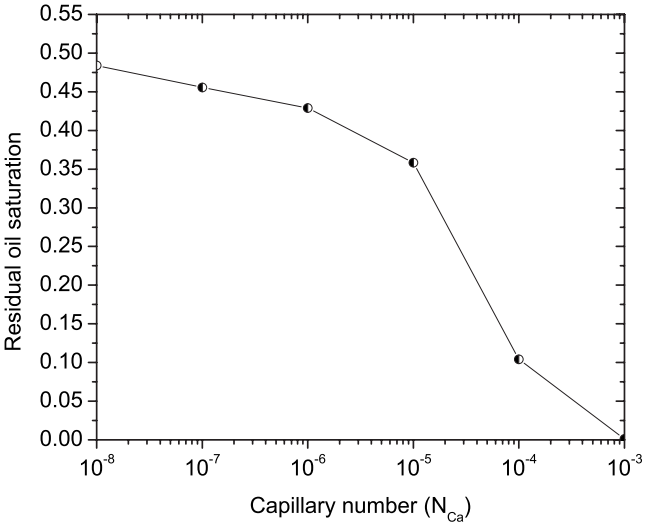

(a) Residual oil saturation

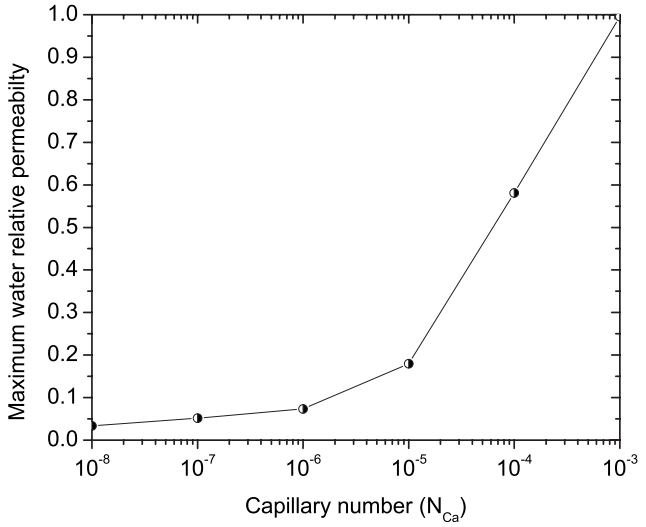

(b) Maximum water relative permeability

FIG. 8. Modeling results—effects of capillary number on the residual oil saturation and maximum water relative permeability of quasidynamic imbibition using map C (see Table II in Ref. [10]) with $S_{wi}=0.024$, $\lambda=2940$, and $\zeta=0°$.

The maximum water relative permeability increases when the capillary number is increased. This is because the residual oil saturation is lower for higher capillary numbers providing more water-filled elements to conduct water through the network. Trapped oil clusters block the flow of water at high residual oil saturations reducing water relative permeability significantly. One should note that the maximum water relative permeability for the capillary dominated imbibition, see Fig. 6(a), is greater than that of $N_{Ca}=1\times10^{-8}$ shown in Fig. 8(b). This is mainly because during the capillary dominated simulations the thickness of the wetting layers is adjusted according to the reduction in capillary pressure, which contributes to the increase in the water relative permeability. This does not take place in quasidynamic

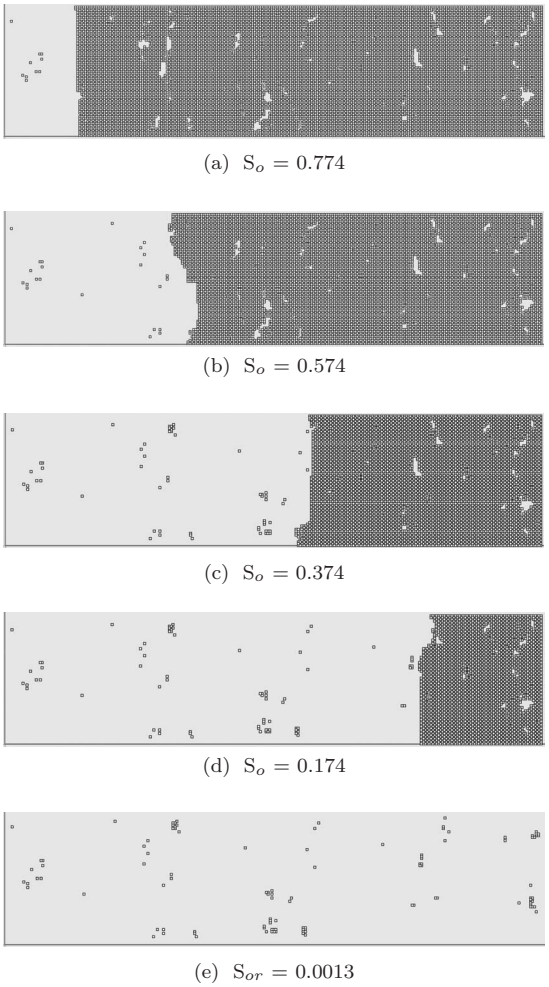

(a) $S_o = 0.774$

(b) $S_o = 0.574$

(c) $S_o = 0.374$

(d) $S_o = 0.174$

(e) $S_{or} = 0.0013$

FIG. 9. Modeling results—fluid occupancy at different oil saturations during quasidynamic imbibition using maps C (see Table II in Ref. [10]) with $N_{Ca}=1\times10^{-3}$, $S_{wi}=0.024$, $\lambda=2940$, and $\zeta=0°$. The dark gray elements are occupied by the defending phase (oil) while the light gray areas include elements that are fully saturated with the invading phase (water).

simulations of imbibition because we assign a fixed conductance to the wetting layers.

C. Gravity effects

Effects of gravity on the fluid occupancy, residual oil saturation, and maximum water relative permeability are studied. The angle that the central plane, along the length, of the fracture makes with the horizontal is labeled ζ. In order to study the effects of gravity, ζ is varied from −90° to +90° in 45° increments. Imbibition simulations were carried out with a low capillary number, $N_{Ca}=1\times10^{-7}$. The initial water saturation was identical to that of Sec. III B. This allows us to study the competition between gravity and capillary forces while the water pressure drop is small. Figure 10 demonstrates how gravity may affect the flow patterns generated by imbibition. Figure 10(c) shows a case where gravity does not contribute to the flow; this is identical to the case depicted in Fig. 7(e).

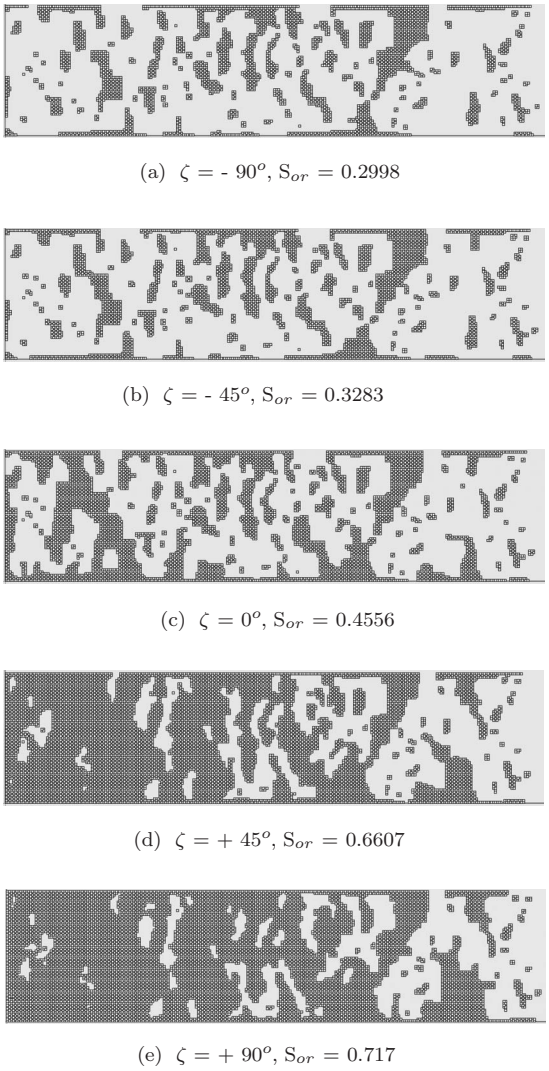

(a) $\zeta = -90^o$, $S_{or} = 0.2998$

(b) $\zeta = -45^o$, $S_{or} = 0.3283$

(c) $\zeta = 0^o$, $S_{or} = 0.4556$

(d) $\zeta = +45^o$, $S_{or} = 0.6607$

(e) $\zeta = +90^o$, $S_{or} = 0.717$

FIG. 10. Modeling results—effects of gravity on the residual oil saturation of quasidynamic imbibition at a constant capillary number (N_{Ca}). Fluid occupancy at residual oil saturation for different values of ζ using map C (see Table II in Ref. [10]) with $S_{wi}=0.024$, $\lambda=2940$, and $N_{Ca}=1\times10^{-7}$. The dark gray elements are occupied by the defending phase (oil) while the light gray areas include elements that are fully saturated with the invading phase (water).

When $\zeta=-90°$, water is injected at the bottom of the fracture flowing upwards to displace oil. In this case, invasion of water into oil in elements away from the inlet is less likely even if threshold capillary pressures are favorable. This means that water will displace oil in a manner that is similar to higher capillary numbers, e.g., $N_{Ca}=1\times10^{-5}$, see Fig. 7(c), leaving large oil-filled elements uninvaded. The threshold oil-water capillary pressure associated with water invasion into oil in large elements is small, thus hindering displacement in those elements. The process results in a residual oil saturation of about 30%; see Fig. 10(a).

If the fracture is rotated 180°, i.e., $\zeta=+90°$, water will flow downwards displacing oil. In this case, gravity will favor displacement of oil residing in elements away from the

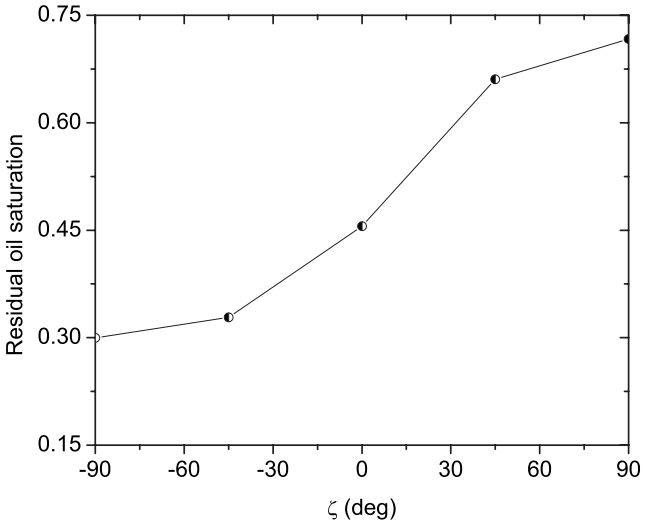

(a) Residual oil saturation

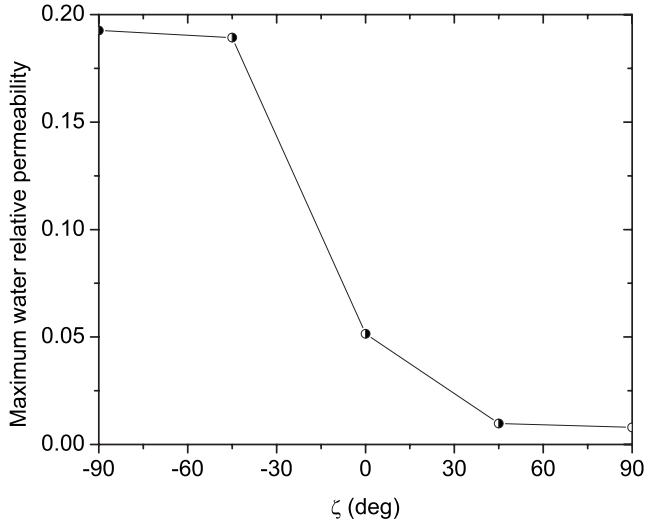

(b) Maximum water relative permeability

FIG. 11. Modeling results—effects of gravity on the residual oil saturation and maximum water relative permeability of quasidynamic imbibition using map C (see Table II in Ref. [10]) with S_{wi} =0.024, λ=2940, and $N_{Ca}=1\times10^{-7}$.

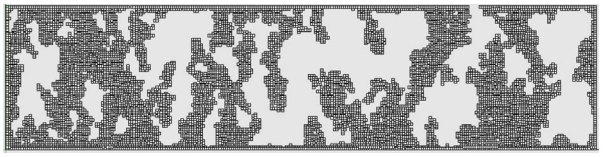

(a) Modeling results: primary drainage at $S_w = 0.35$. This is the initial condition for imbibition results shown in (12(b)) and (12(c)).

(b) Modeling results: capillary dominated imbibition with $S_{wi} = 0.35$ and S_{or}=0.4489.

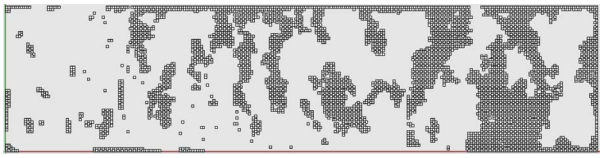

(c) Modeling results: quasidynamic imbibition including rate and gravity effects with $\zeta = -90^{o}$, λ=10371, ΔP_w=1460 Pa, S_{wi}=0.35, $S_o = 0.3707$.

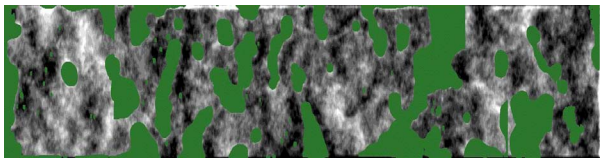

(d) (Color online) Experiment, $S_{wi} = 0.35$ and $S_o = 0.37$.

FIG. 12. (Color online) Comparison against the experiment (imbibition)—experimental and predicted fluid occupancies. Predicted fluid occupancies [(b) to (d)] were generated using map C (see Table II in Ref. [10]). The dark gray elements are occupied by oil while the light gray areas include elements that are fully saturated with water.

inlet increasing the possibility of trapping large clusters of oil. Figure 10 also depicts fluid occupancy for cases with intermediate values of ζ. Residual oil saturation increases by increasing ζ. Figure 11 shows the variation in residual oil saturation and maximum water relative permeability with ζ.

D. Comparison with the experiment

All the available experimental parameters are used in the model to simulate imbibition. Predicted fluid occupancy is compared with its experimental counterpart. Capillary, rate, and gravity effects are taken into account (quasidynamic). During each step of the experiment, the invading fluid was injected from the bottom of the core flowing upwards to displace the defending phase, i.e., $\zeta=-90°$. Initial water saturation for imbibition was S_{wi}=0.35 and final oil saturation, when the scanning was initiated, was about S_o=0.37. Quasidynamic simulations were carried out with $N_{Ca}=1.7\times10^{-5}$ which was calculated using Eq. (1) with Q_w=0.5 cc/min, μ_w=1.2 cP, $\bar{a}$=0.5817 mm, R_w=0.3281 mm, N_w=75, and σ_{ow}=41.2 mN/m. Unfortunately pressure drop was not measured during the experiment. This means that we were not able to adjust parameter λ to reproduce an experimentally measured pressure drop. However, we believe, based on our experience in performing similar experiments, a pressure drop of about 1460 Pa, achieved at λ=10371, is plausible. Small changes in parameter λ did not affect the results adversely.

Figure 12 compares the top view of fluid occupancy predicted by the model with the one that was generated using

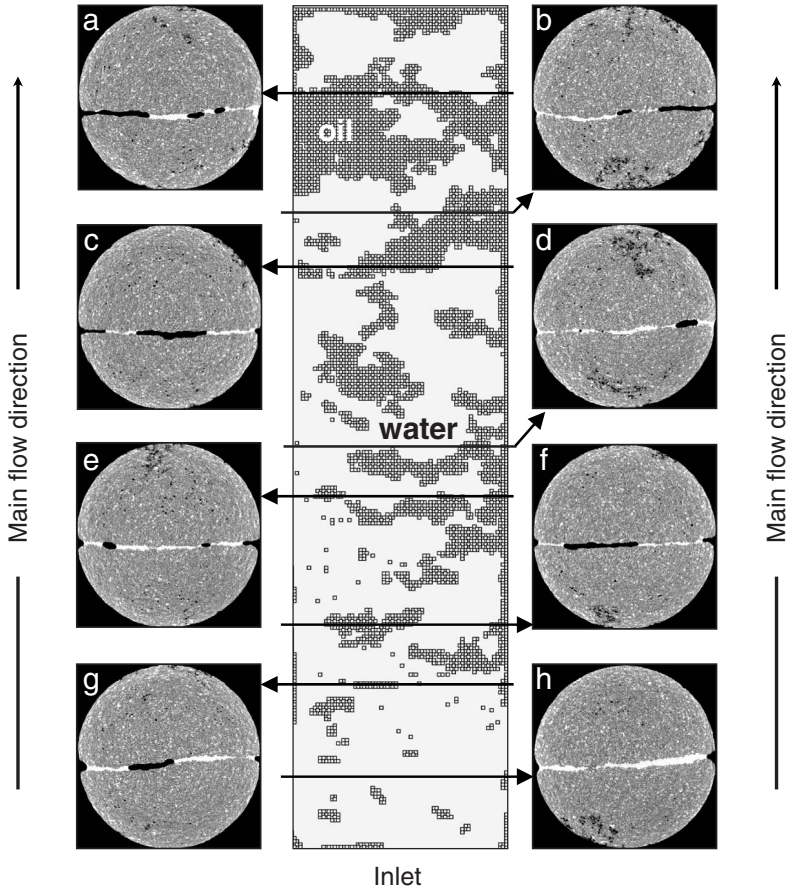

FIG. 13. Comparison against the experiment (quasidynamic imbibition)—comparison of predicted fluid occupancy against experimental CT slices at $S_o \approx 0.37$, using map C (see Table II in Ref. [10]). Distance from the bottom, or inlet, of the core: (a) 91.07 mm; (b) 76.91 mm; (c) 70.89 mm; (d) 48.60 mm; (e) 42.83 mm; (f) 27.24 mm; (g) 20.05 mm; (h) 8.85 mm. In the predicted fluid occupancy, dark gray elements are occupied by the invading phase (water) while the light gray areas include elements that are fully saturated with the defending phase (oil). In the CT slices, white represents water while black represents oil.

x-ray imaging at the end of stage 4 of the experiment, see Ref. [10]. Figure 12(a) shows fluid occupancy at $S_w=0.35$ due to capillary dominated primary drainage. This provided the initial condition for imbibition.

Figures 12(b) and 12(c) present fluid occupancy for capillary dominated and quasidynamic modeling of imbibition. Capillary dominated simulation gives a residual oil saturation of $S_{or}=0.4489$ which is greater than the oil saturation measured at the end of stage 4 of the experiment, $S_o=0.37$. But since quasidynamic simulation leads to lower residual oil saturation we were able to terminate the simulation at $S_o=0.3707$, before reaching residual oil saturation. Even though that capillary dominated simulation leads to higher oil saturation than the experiment, still it is evident that taking rate and gravity effects into account produces greater similarities between the predicted fluid occupancy and the x-ray image. For instance, the large cluster of water-filled elements, shown in the left side of the x-ray image, see Fig. 12(d), has not been reproduced by the capillary dominated simulation, see Fig. 12(b), while quasidynamic simulation, see Fig. 12(c), does reproduce the cluster to great extent. This is also the case for another relatively large water-filled cluster located at the right side of the x-ray image. Quasidynamic model reproduces the cluster successfully while the capillary dominated simulation does not. Despite the improvements in the prediction of fluid occupancy, there are locations where the quasidynamic model fails to reproduce the correct fluid residence. This could be due to the fact that we ignore the pressure drop in the nonwetting phase and also assign a fixed conductance to the wetting layers. Fully dynamic models do not make such assumptions but are much more expensive computationally, particularly in high capillary number cases.

Similar to primary drainage, we present a rigorous comparison of fluid occupancy for imbibition. Figure 13 compares predicted fluid occupancy for eight different locations along the length of the fracture with their experimental counterparts shown by the CT slices. Despite the assumptions made, the agreement is very good. There are, however, locations where the predicted fluid occupancy disagrees with the experiment but the improvement in the predicted fluid occupancy is significant when compared to the one generated by the capillary dominated simulation.

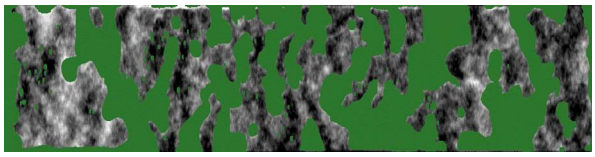

(a) (Color online) Experiment with $S_{wi}=0.63, S_o = 0.58$.

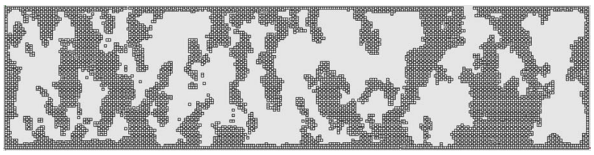

(b) Capillary dominated secondary drainage with $S_{wi}=0.6293$, $S_o=0.5797$.

FIG. 14. (Color online) Comparison against the experiment (capillary dominated secondary drainage)—experimental and predicted fluid occupancies at $S_o \approx 0.58$. Predicted fluid occupancy shown in subfigure (b) was generated using map C (see Table II in Ref. [10]). The dark gray elements are occupied by the invading phase (oil) while the light gray areas include elements that are fully saturated with the defending phase (water).

IV. SECONDARY DRAINAGE

In this section we assume that stage 5 of the experiment, see Table I in Ref. [10], where oil and water were injected simultaneously, can be represented by secondary capillary dominated oil injection. Capillary dominated secondary oil drainage was conducted into water after quasidynamic imbibition. Initial oil saturation was $S_{oi}=0.3707$, similar to the oil saturation at the end of stage 4 of the experiment. The initial condition is depicted in Fig. 12(c). In order to account for the increase in water pressure during imbibition, oil-water capillary pressure was reduced to 20% of P_{cow}^{PD} in the beginning of secondary oil injection. P_{cow}^{PD} is the maximum oil-water capillary pressure reached during primary drainage. One should note that since this is a capillary dominated process, small changes in the percentage of reduction in oil-water capillary pressure prior to secondary oil injection did not affect the results significantly.

Then, oil was injected to reduce water saturation to $S_w = 0.42$ which is the water saturation measured at the end of stage 5 of the experiment. Figure 14 compares the top view of fluid occupancy predicted by the model against the corresponding x-ray image. The agreement is excellent. A careful

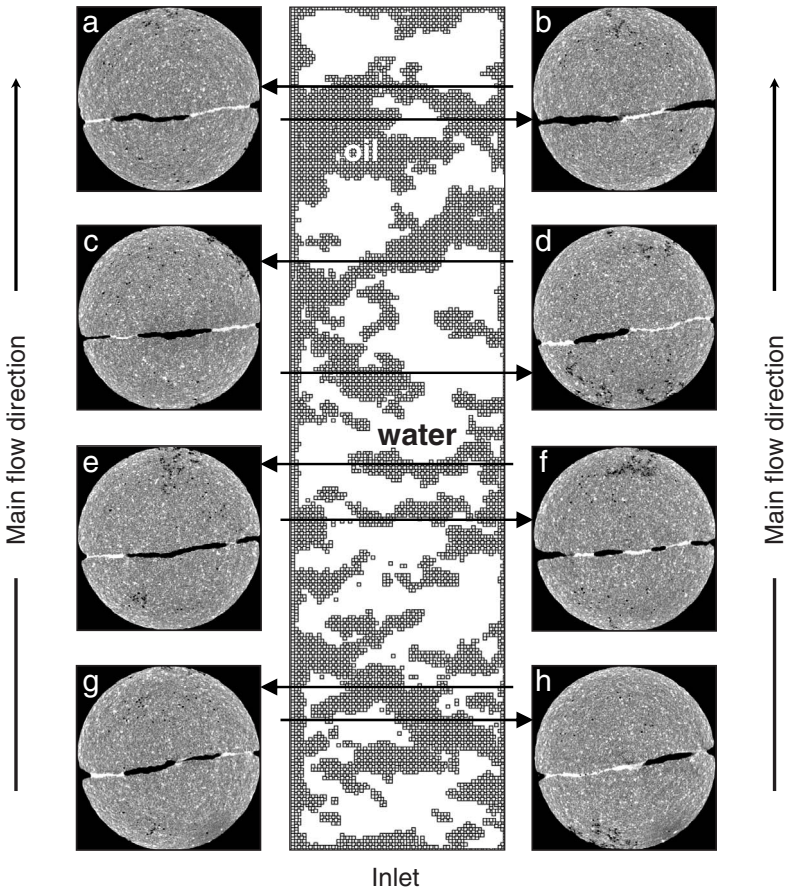

FIG. 15. Comparison against the experiment (capillary dominated secondary drainage)—comparison of predicted fluid occupancy against experimental CT slices at $S_o \approx 0.58$, using map C (see Table II in Ref. [10]). Distance from the bottom, or inlet, of the core: (a) 92.20 mm; (b) 88.46 mm; (c) 71.18 mm; (d) 56.63 mm; (e) 46.35 mm; (f) 39.74 mm; (g) 19.96 mm; (h) 15.08 mm. In the predicted fluid occupancy, dark gray elements are occupied by the invading phase (oil) while the light gray areas include elements that are fully saturated with the defending phase (water). In the CT slices, white represents water while black represents oil.

examination shows that most of the features shown by the x-ray image have been reproduced by the model. The assumption that simultaneous injection of oil and water is a capillary dominated oil invasion process is thus valid.

Figure 15 shows a comparison of predicted fluid occupancy at eight different locations along the length of the fracture with the experimental fluid occupancy depicted by the CT slices at the same locations. Again the agreement is excellent.

V. CONCLUDING REMARKS

The conceptual network model of connected pores and throats, described in paper I [10], has been successfully implemented and rigorously validated against experimental findings. Transport properties, such as fracture permeability, relative permeability, and capillary pressure, were systematically computed and fluid structures compared against experimental results. Through detailed description of experimental conditions we were able to predict fluid distributions for a fracture whose geometry had been mapped using x-ray microtomography. This indicates that the application of a deterministic physically-based tool is appropriate to predict fluid distributions in realistic fracture representations.

Both primary and secondary drainage results revealed excellent agreement with x-ray CT slices showing fluid occupancy at various fracture locations. These results support the validity of the capillary dominated assumption imposed in the modeling of primary and secondary drainage. Bridges of nonwetting phase formed during primary drainage were found to have a strong effect on the ability of the fracture to conduct water, which is illustrated as a sharp decrease in water relative permeability. Three networks representing the fracture inner structure at various levels of resolution showed similar results, while a fourth map with a further reduction in resolution started to exhibit deviations from the previous accurate representation of fluid structures.

Imbibition was studied using two approaches, capillary dominated and quasidynamic flow for which rate and gravity effects were taken into account. In general, snapoff did not play a major role in developing fluid flow patterns during imbibition, while cooperative pore filling was the dominant displacement mechanism. Varying the capillary number allowed us to depict different imbibition scenarios where capillarity and viscous forces had different relative influence. At high capillary numbers, viscous forces were dominant and there was less chance for oil trapping in the fracture. This consequently led to lower residual oil saturation and higher maximum water relative permeability.

The effect of gravity on the resulting fluid structures was examined at a low capillary number through changes in fracture inclination with respect to a horizontal reference. At -90° inclination, water injection takes place in the upward direction and local displacement resembles flow at greater capillary numbers, reducing the chance for oil trapping. At $+90^\circ$ inclination, water injection takes place in the downward direction, which makes the displacements away from the inlet competitive with those that are closer to the inlet. This enhanced the chance for oil trapping. The residual oil saturation in the fracture increased with the angle of inclination. Comparison of predicted fluid flow structures, for imbibition, with those reported experimentally showed good agreement when rate and gravity effects were taken into account.

ACKNOWLEDGMENTS

The Enhanced Oil Recovery Institute of the University of Wyoming and the Center for Quantitative Imaging at the Pennsylvania State University are gratefully thanked for their support. We also thank R. G. Hughes (Louisiana State University), M. J. Blunt (Imperial College London), and A. S. Grader (the Pennsylvania State University) for valuable discussions.

[1] J. de la Porte, C. Kossack, and R. Zimmerman, in Paper SPE 95241, Proceedings of the SPE Annual Technical Conference and Exhibition, Dallas, Texas (2005).
[2] A. Dicman, E. Putra, and D. S. Schechter, in Paper SPE 89442, Proceedings of the SPE/DOE Symposium on Improved Oil Recovery, Tulsa, Oklahoma (2004).
[3] J. R. Gilman and H. Kazemi, SPEJ **8**, 695 (1983).
[4] J. E. Warren and P. J. Root, SPEJ **9**, 245 (1963).
[5] R. E. Guzman and K. Aziz, in Paper SPE 24916, Proceedings of the 67th SPE Annual Technical Conference and Exhibition, Washington, D.C. (1992).
[6] E. S. Romm, *Fluid Flow in Fractured Rocks* (Phillips Petroleum Co., Bartlesville, OK, 1972), English translation.
[7] Y. W. Tsang, Water Resour. Res. **20**, 1209 (1984).
[8] W. R. Rossen and A. T. A. Kumar, in Paper SPE 28700, Proceedings of the SPE Intametionel Petroleum Conference and Exhibition of Mexico, Veracruz, Mexico (1994).
[9] D. A. Pieters and R. M. Graves, in Paper SPE 28701, Proceedings of the SPE Intametionel Petroleum Conference and Exhibition of Mexico, Veracruz, Mexico (1994).
[10] Z. T. Karpyn and M. Piri, preceding paper, Phys. Rev. E **76**, 016315 (2007).
[11] D. Wilkinson and J. F. Willemsen, J. Phys. A **16**, 3365 (1983).
[12] Z. T. Karpyn, A. S. Grader, and P. M. Halleck, J. Colloid Interface Sci. **307**, 181 (2007).
[13] R. G. Hughes and M. J. Blunt, Adv. Water Resour. **24**, 409 (2001).